Magnetic hysteresis of individual Janus particles with hemispherical exchange biased caps ⓕ

S. Philipp,[1] ⓘ B. Gross,[1] M. Reginka,[2] ⓘ M. Merkel,[2] ⓘ M. M. Claus,[1] ⓘ M. Sulliger,[1] ⓘ A. Ehresmann,[2] ⓘ
and M. Poggio[1,3,a] ⓘ

AFFILIATIONS

[1]Department of Physics, University of Basel, 4056 Basel, Switzerland
[2]Institute of Physics, University of Kassel, 34132 Kassel, Germany
[3]Swiss Nanoscience Institute, University of Basel, 4056 Basel, Switzerland

[a]Author to whom correspondence should be addressed: martino.poggio@unibas.ch

ABSTRACT

We use sensitive dynamic cantilever magnetometry to measure the magnetic hysteresis of individual magnetic Janus particles. These particles consist of hemispherical caps of magnetic material deposited on micrometer-scale silica spheres. The measurements, combined with corresponding micromagnetic simulations, reveal the magnetic configurations present in these individual curved magnets. In remanence, ferromagnetic Janus particles are found to host a global vortex state with vanishing magnetic moment. In contrast, a remanent onion state with significant moment is recovered by imposing an exchange bias to the system via an additional antiferromagnetic layer in the cap. A robust remanent magnetic moment is crucial for most applications of magnetic Janus particles, in which an external magnetic field actuates their motion.

Published under an exclusive license by AIP Publishing. https://doi.org/10.1063/5.0076116

Janus particles (JPs) are nano- or micronsized particles that possess two sides, each having different physical or chemical properties. There is a multitude of types of JPs,[1] differing in shape, material, and functionalization. As a subgroup of micrometer and sub-micron sized magnetic particles, which are discussed as a multi-functional component in lab-on-chip or micro-total analysis systems,[2,3] magnetic JPs consist of a hemispherical cap of magnetic material on a non-magnetic spherical template. Such JPs can be mass-produced via the deposition of magnetic layers on an ensemble of silica spheres. The transversal and rotary motion of these particles can be controlled via external magnetic fields, which exert magnetic forces and torques.[4–6] This ability to externally actuate magnetic JPs has led to applications in microfluidics, e.g., as stirring devices,[7] as microprobes for viscosity changes,[8] or as cargo transporters in lab-on-chip devices.[9–11] Magnetic JPs have also been proposed as an *in vivo* drug delivery system.[12]

Although, in general, a transversal controlled motion can be achieved by both superparamagnetic particles or particles with a permanent magnetic moment, a control over the rotational degrees of freedom can only be achieved, if the particles possess a sufficiently large permanent magnetic moment. Streubel *et al.*[13] analyzed the remanent magnetic state of magnetic JPs with ferromagnetic (fm) magnetic caps. Their simulations show that Permalloy JPs with diameters

larger than 140 nm host a global vortex state at remanence. Because this flux-closed state has a vanishing net magnetic moment, magnetic JPs hosting such a remanent configuration are unsuited for applications involving magnetic actuation. Thus, for JPs larger than this critical diameter, strategies to overcome this limitation need to be developed.

Here, we make use of exchange bias,[14–16] which, in a simplified picture, imposes a preferred direction on the magnetic moments of the fm layer and is, therefore, able to prevent the formation of a global vortex at remanence. We apply an exchange bias to the fm layer by adding an antiferromagnetic (afm) layer beneath the fm layer. In order to verify that this addition leads to a remanent configuration with large magnetic moment, we measure the magnetic hysteresis of individual JPs with and without this layer. The measurement of individual JPs is necessary in order to eliminate the effects of interactions between neighboring JPs. For this task, we employ dynamic cantilever magnetometry (DCM) and analyze the results by comparison with corresponding micromagnetic simulations. This technique overcomes the limitation of earlier measurements that were restricted to ensembles of interacting JPs on a substrate.[17] Those measurements relied on the longitudinal magneto-optical Kerr effect and magnetic force microscopy. They found an onion state with a large remanent magnetization

in JPs with an afm layer. For the onion state, magnetic moments align tangentially to the cap's surface following its curvature while the macroscopic net moment points along the exchange bias (and hence magnetic easy) direction. Nevertheless, given that the measurements were done on close-packed ensembles of JPs, they do not exclude effects due to the interaction between the particles and, therefore, cannot be used to infer the behavior of isolated JPs.

We fabricate the magnetic JPs by coating a self-assembled template of $1.5\,\mu m$-sized silica spheres with thin layers of different materials via sputter-deposition. The non-magnetic silica spheres are arranged on a silica substrate using entropy minimization,[18] which allows the formation of hexagonal close-packed monolayers. JPs with two different layer stacks, shown in Fig. 1(b), are produced. Ferromagnetic JPs (fmJPs) are fabricated by depositing a 10 nm-thick Cu buffer layer directly on the silica spheres, followed by a 10 nm-thick layer of ferromagnetic CoFe. The film is sealed by a final 10 nm-thick layer of Si. A second type of JP, which we denote exchange-bias JPs (ebJPs), includes an additional 30 nm-thick afm layer of $Ir_{17}Mn_{83}$ between the Cu buffer and the fm layer. Layer deposition is performed by sputtering in an external magnetic field of 28 kA/m applied in the substrate plane, i.e., in the equatorial plane of the JPs, in order to initialize the exchange bias by field growth. This fabrication process is described in detail in Tomita et al.[17] Individual JPs are then attached to the apex of a cantilever for magnetic characterization in a last fabrication step, as shown in the scanning electron micrographs (SEMs) of Figs. 2(a) and 2(b).

Note that the values given for thicknesses are nominal and that the film thickness gradually reduces toward the equator of the sphere
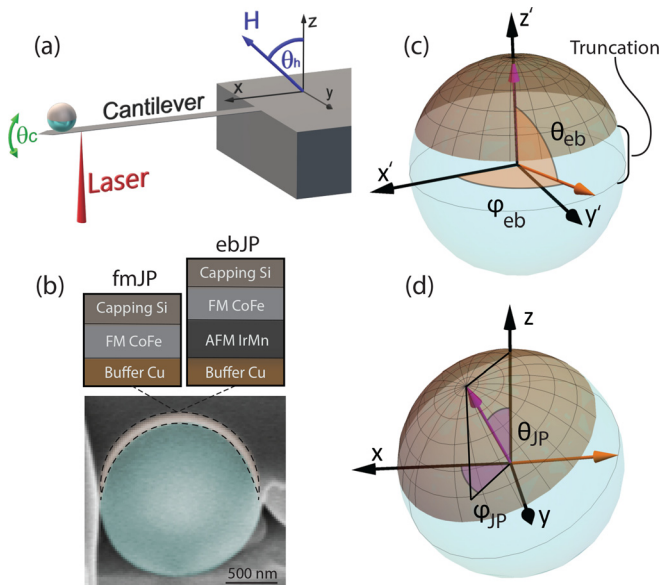
FIG. 1. (a) Sketch of a cantilever with a JP attached to its tip and definition of the coordinate system. (b) Cross-sectional SEM of a JP showing the gradient of the layer thickness. The two investigated layer stacks of the hemispherical cap are shown in the insets. (c) and (d) Sketches of a microsphere showing the surface area of the magnetic layer (brown, meshed area) as used in simulation, including the truncation. Definition of the angles setting the orientation of the unidirectional anisotropy vector used to mimic exchange bias effects (θ_{eb}, φ_{eb}) and the angles defining the orientation of a JP on the cantilever (θ_{JP} and φ_{JP}).
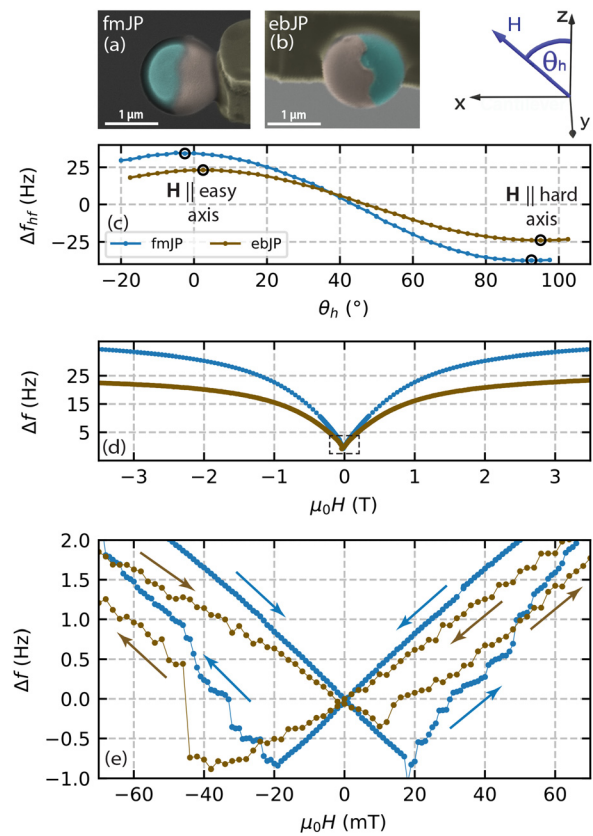
FIG. 2. False color SEMs of the (a) fmJP and (b) ebJP attached to the tip of a cantilever, respectively. The coordinate system is shown on the right. (c) $\Delta f_{hf}(\theta_h)$ measured at $\mu_0 H = 3.5\,T$ for the fmJP (blue) and ebJP (brown). Black circles indicate θ_h of the hysteresis measurements, which are shown in (d) and (e) and Fig. 3. Note that differences in the noise level of the data in (e) originate in different measurement settings and do not have physical origin.

with respect to the top, as shown in Fig. 1(b), because of the deposition process.[17] Furthermore, the touching points of the next neighbors in the hexagonal closed packed arrangement of the silica spheres on the substrate template impose a lateral irregularity on the equatorial line of the capping layers. This is best seen in Figs. 2(a) and 2(b).

We measure the magnetic hysteresis of an individual fmJP and an individual ebJP via DCM. DCM is a technique to investigate individual, nano- to micrometer-sized magnetic specimens, similar to a standard vibrating superconducting quantum interference device (SQUID) magnetometer. The key differences are that DCM is sensitive enough to measure much smaller magnetic volumes than a vibrating SQUID magnetometer and that it measures magnetic properties with respect to rotations of the external magnetic field, rather than modulations of its amplitude as in measurements of magnetic susceptibility. Details on the technique and measurement setup can be found in Refs. 19 and 20.

A magnetic specimen is attached to the tip of a cantilever, which is driven in a feedback loop at its resonance frequency f with a fixed amplitude, actuated by a piezoelectric transducer. A uniform external magnetic field **H** is applied to set the magnetic state of the specimen

under investigation. **H** can be rotated within the plane perpendicular to the cantilever's rotation axis (xz-plane) with a span of $117.5°$ and a maximum field amplitude of $H = \pm 3.5\,\text{T}$. Its orientation is set by the angle θ_h as defined and indicated in Fig. 1(a). The magnetic torque acting on the sample results in a deflection of the cantilever as well as a shift in its resonance frequency, which is given by

$$\Delta f = f - f_0 = \frac{f_0}{2k_0 l_e^2}\left(\frac{\partial^2 E_m}{\partial \theta_c^2}\Big|_{\theta_c=0}\right), \qquad (1)$$

where f_0 and k_0 are the resonance frequency and spring constant of the cantilever at zero applied field, respectively, l_e is the effective length of the cantilever, θ_c is the oscillation angle, and E_m is the magnetic energy of the specimen. Properties of the cantilevers used in the experiments can be found in Sec. I of the supplementary material.

In the limit of large applied magnetic field, such that the Zeeman energy dominates over the anisotropy energy, all magnetic moments align along **H**. In this limit, Δf asymptotically approaches a value determined by the involved anisotropies, their respective directions, the total magnetic moment, θ_h, and the mechanical properties of the cantilever.[19,20] In particular, the determination of these asymptotes allows us to extract the direction of magnetic easy and hard axes by measuring the angular dependence of the frequency shift at high field Δf_{hf}. The maximum positive (minimum negative) $\Delta f_{\text{hf}}(\theta_h)$ indicates the easy (hard) axis. For these measurements, shown in Fig. 2(c), we apply $\mu_0 H = 3.5\,\text{T}$, which we expect to be in the high field limit. See Secs. VI and VII of the supplementary material for more details. We also measure the magnetic hysteresis of $\Delta f(H)$ by sweeping the applied field H up and down for θ_h fixed to the values determined for the magnetic easy and hard axes, respectively. This procedure reveals signatures of the JPs' magnetic reversal, as shown in Figs. 2(d), 2(e), and 3.

In order to analyze both these types of measurements, we perform micromagnetic simulations using the finite-element software Nmag.[21] We calculate $\Delta f(H)$ from the micromagnetic state for parameters set by the experiment.[19,22] Matching these simulations to the measurements gives us a detailed understanding of the progression of the magnetic configurations present in the JPs throughout the reversal process. Events, such as the nucleation of a magnetic vortex, can be identified and associated with features in $\Delta f(H)$ measured via DCM.

Figures 2(a) and 2(b) show false color SEMs of the measured fmJP and ebJP, respectively, each attached to the tip of a cantilever. The orientation of the particles in the images can be correlated with the angle θ_h of the maxima and minima found in the high-field frequency shift $\Delta f_{\text{hf}}(\theta_h)$ in dependence of the magnetic field angle θ_h, shown in Fig. 2(c). Doing so, we find a magnetic easy direction in the equatorial plane of the particles and a hard direction along the axis of the pole. The $90°$ angle between easy and hard direction is a clear indication that uniaxial anisotropy is the dominant anisotropy in the system. We ascribe the latter to the shape of the JPs, because no other strong anisotropies are expected.

The field-dependent frequency shift $\Delta f(H)$ for **H** aligned along the easy axis, see Fig. 2(d), shows a typical hysteretic, V-shaped curve, that approaches a horizontal asymptote for high field magnitudes.[19] The fmJP shows a symmetric asymptotic behavior for $\mu_0 H = 3.5\,\text{T}$ and $-3.5\,\text{T}$ (blue curve). Magnetic reversal at low fields, $\mu_0 H$ around $\pm 20\,\text{mT}$, is symmetric upon reversal of the field sweep direction, as
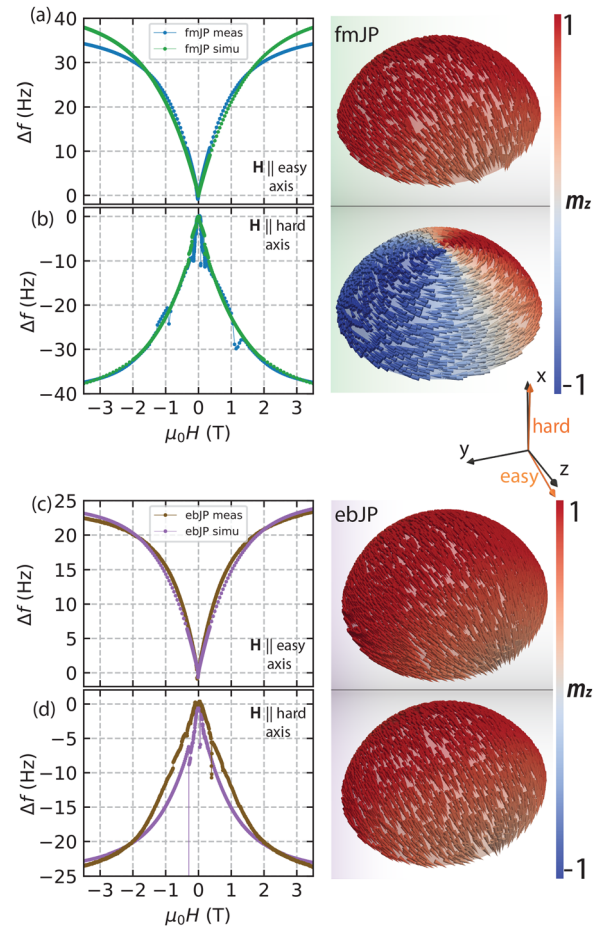
FIG. 3. Measured and simulated $\Delta f(H)$ of the fmJP for **H** applied along the (a) easy and (b) hard axis, respectively. A visualization of each corresponding simulated remanent magnetic state is shown on the right. The same set of data for the ebJP is shown in (c) and (d).

shown in Fig. 2(e). This behavior is expected for a ferromagnetic particle with a magnetic field applied along its easy axis.

In contrast, measurements of the ebJP reveal asymmetric asymptotic behavior with Δf_{hf} values differing by about $0.9\,\text{Hz}$ for $\mu_0 H = \pm 3.5\,\text{T}$, as seen in the brown curve of Fig. 2(d). Furthermore, after a full hysteresis cycle, we observe a reduction in the difference of Δf_{hf} at $\pm 3.5\,\text{T}$ by about $0.4\,\text{Hz}$, which is evidence for magnetic training.[23,24] Measurements of the ebJP also show a highly asymmetric magnetic reversal, which occurs at $\mu_0 H = -44\,\text{mT}$ when sweeping the field down and at $\mu_0 H = 12\,\text{mT}$ when sweeping the field up. All of these findings are characteristic of an exchange bias imposed on the fm layer by the afm layer.

In order to draw conclusions about the magnetic state of the JPs, we establish a micromagnetic model for each of the two types of JPs over many iterations of comparison to measured $\Delta f(H)$ and variations of the parameters for **H** applied along the magnetic easy and hard axis, respectively. This iterative process, information from the literature, and observations from SEMs lead to a final set of parameters

(see the supplementary material, Sec. I) and a model that reproduces the measured $\Delta f(H)$. The model assumes that the magnetic JPs are made from a hemispherical shell with a thickness gradient from the pole toward the equator, which accounts for the gradual reduction in the shell thickness away from the pole, as shown in Fig. 1(b). The hemisphere is also truncated[25] by a latitudinal belt around the equator, reflecting observations from the SEM images in Figs. 2(a) and 2(b). For simplicity, in the simulations, we do not account for the magnetic film's irregular edge at the equator and a possible change in the crystallographic texturing with respect to the particle surface as a function of position within the cap. The orientation of a JP with respect to the cantilever rotation axis and $\mathbf{H}$ is set by inferring the orientation from the SEMs and followed by an iterative tuning of the angles $(\theta_{JP}, \varphi_{JP})$, as defined in Fig. 1(d), to match the measured $\Delta f(H)$.

Figures 3(a) and 3(b) show agreement between the measured and simulated $\Delta f(H)$ curves for the fmJP for $\mathbf{H}$ applied along the magnetic easy and hard axis, respectively. The overall shape of the latter is mostly a mirrored image of the V-shape for easy axis alignment at the field axis. This shape is a peculiarity arising from the curved geometry and opposes to the typical Stoner–Wohlfarth-like shape found for easy plane anisotropy, see the supplementary material, Secs. III and IV. Similar curves are shown for the ebJP in Figs. 3(c) and 3(d). Details on the progression of the magnetization configurations as a function of H, as indicated by the simulations, are found in Sec. II of the supplementary material. Here, we focus on the remanent magnetization configurations in both types of particles, as shown on the right of Fig. 3.

For the fmJP, an onion state is realized after sweeping $\mathbf{H}$ along the easy axis while a global vortex state is found after sweeping $\mathbf{H}$ along the hard axis. In applications, magnetic JPs are subject to considerable disturbances from the outside, including thermal activation, interactions with other nearby magnetic particles, and alternating external magnetic fields for actuation. Hence, we can expect a magnetic JP to relax to its ground state configuration over time. The simulation of the fmJP shows that when the magnetization is in the global vortex state, its magnetic energy is 101 aJ lower than when it is in the onion state. The global vortex state is, therefore, energetically more favorable than the onion state, which is also true if compared to any other remanent state that we have found in simulations for fmJPs, as discussed in the supplementary material, Sec. IV. This analysis suggests that a remanent global vortex state, which has a vanishing total magnetic moment, is realized in fmJPs over time, independent of magnetic history. If we normalize the magnetic moment of this state by the saturation moment, $M_s V$, we find that the global vortex state hosted by the fmJP has a moment value of 0.03, precluding the use of such particles in applications. (For completeness, the normalized magnetic moment of the onion state has a value of 0.64.)

We establish a similar micromagnetic model for the ebJP. To model the effect of an exchange bias imposing a preferred direction on the magnetic moments in the ferromagnet, a unidirectional anisotropy is added to the simulation. Note that other influences of the afm layer are not accounted for, especially contributions to the coercive field,[26] rotational anisotropies,[27] or contributions arising due to its granular structure.[28] For this reason, neither the asymmetric values of the magnetic reversal fields nor the observed training effects are correctly reproduced by the simulation. The unidirectional anisotropy, described by a unit vector $\hat{\mathbf{u}}_{eb}$ with orientation angles $(\theta_{eb}, \varphi_{eb})$, as shown in Fig. 1(c), and an anisotropy constant K_{eb}, is expected to lie

somewhere in the equatorial plane of the ebJP. The specific orientation of $\hat{\mathbf{u}}_{eb}$ within this plane is induced in the afm by the magnetic field applied during deposition. Note that for simplicity, K_{eb} is kept constant within the whole volume of the magnetic cap, despite thickness variations of the afm layer with θ_{eb}.

The knowledge of where $\hat{\mathbf{u}}_{eb}$ points within the equatorial plane is lost after attaching the JP to the cantilever. In the simulations, we choose to align $\hat{\mathbf{u}}_{eb}$ along the direction in the equatorial plane that coincides with the applied external field in the easy-axis configuration, even though it could point along any direction in this plane. This assumption that $\mathbf{H}$ and $\hat{\mathbf{u}}_{eb}$ are collinear in the easy-axis measurements means that our simulations predict the maximum possible Δf for any given choice of the unidirectional anisotropy constant K_{eb} and, hence, give a lower bound for K_{eb}.

We adjust this anisotropy to match the measured $\Delta f(H)$ along both the easy and hard axes and find good agreement for $K_{eb} = 22.5\,\mathrm{kJ/m^3}$. In particular, the model reproduces the asymmetry in Δf_{hf} for both the easy and hard-axis alignments, as shown in Figs. 3(c) and 3(d). This value of K_{eb} is also consistent with results from Ref. 28, once the influence of a reduced sample size is considered.[29]

At remanence, the simulations show that the ebJP hosts an onion state irrespective of its magnetic history, as shown in Figs. 3(c) and 3(d). To exclude the presence of an equilibrium global vortex state, we test this state's stability by initializing the ebJP in a global vortex state at remanence and then relaxing the system to a local energetic minimum. Following this procedure, the system relaxes to the onion state. As a result, we can exclude the global vortex state as a possible equilibrium remanent state in this ebJP.

For the simulations of the ebJP, we find a total magnetic moment at remanence of 0.89 and 0.71, normalized by its maximum value of $M_s V$, depending on whether $\mathbf{H}$ is applied along the hard or easy direction of the external field, respectively. This remanent moment represents an increase in more than one order of magnitude compared to the remanent moment of the fmJP. Hence, introducing exchange bias to magnetic JPs, if strong enough, succeeds in stabilizing a high-moment onion state in remanence.

To conclude, micrometer-sized JPs capped with an antiferromagnetic/ferromagnetic or purely ferromagnetic thin film system have been mass produced through a sputter-deposition process. We have investigated the magnetic reversal and remanent magnetic configurations of individual specimens of these JPs using DCM and corresponding micromagnetic simulations. Although the fmJPs host a global vortex state in remanence with a vanishing magnetic moment, the addition of an antiferromagnetic layer in ebJPs changes the remanent configuration to a stable high-moment onion state. Unlike previous measurements on close packed particle arrays, our measurements on individual JPs show that the stability of this high magnetic moment texture in remanence is a property of the individual particles and present in the absence of interparticle interactions. A high magnetic moment in remanence allows for rotational and translational control of the JPs, as demonstrated in Ref. 30.

See the supplementary material for information as referred to in the main text.

building the measurement system. They acknowledge the support of the Canton Aargau and the Swiss National Science Foundation under Grant No. 200020-159893, via the Sinergia Grant Nanoskyrmionics (Grant No. CRSII5-171003), and via the National Centre for Competence in Research Quantum Science and Technology. Calculations were performed at sciCORE (http://scicore.unibas.ch/) scientific computing core facility at University of Basel. They further acknowledge Thomas Kusserow, University of Kassel, for his support with the acquisition and imaging of the FIB cut particle cross sections.

AUTHOR DECLARATIONS
Conflict of Interest

The authors have no conflicts of interest to disclose.

DATA AVAILABILITY

The data that support the findings of this study are available from the corresponding author upon reasonable request.

REFERENCES

[1]A. Walther and A. H. E. Müller, "Janus Particles: Synthesis, self-assembly, physical properties, and applications," Chem. Rev. **113**(7), 5194–5261 (2013).

[2]D. Issadore, Y. I. Park, H. Shao, C. Min, K. Lee, M. Liong, R. Weissleder, and H. Lee, "Magnetic sensing technology for molecular analyses," Lab Chip **14**, 2385–2397 (2014).

[3]A. Ehresmann, I. Koch, and D. Holzinger, "Manipulation of superparamagnetic beads on patterned exchange-bias layer systems for biosensing applications," Sensors **15**(11), 28854–28888 (2015).

[4]B. H. McNaughton, K. A. Kehbein, J. N. Anker, and R. Kopelman, "Sudden breakdown in linear response of a rotationally driven magnetic microparticle and application to physical and chemical microsensing," J. Phys. Chem. B **110**(38), 18958–18964 (2006).

[5]B. H. McNaughton, P. Kinnunen, M. Shlomi, C. Cionca, S. N. Pei, R. Clarke, P. Argyrakis, and R. Kopelman, "Experimental system for one-dimensional rotational brownian motion," J. Phys. Chem. B **115**(18), 5212–5218 (2011).

[6]R. M. Erb, J. J. Martin, R. Soheilian, C. Pan, and J. R. Barber, "Actuating soft matter with magnetic torque," Adv. Funct. Mater. **26**(22), 3859–3880 (2016).

[7]G. Steinbach, M. Schreiber, D. Nissen, M. Albrecht, S. Gemming, and A. Erbe, "Anisotropy of colloidal components propels field-activated stirrers and movers," Phys. Rev. Res. **2**(2), 023092 (2020).

[8]K. V. T. Nguyen and J. N. Anker, "Detecting de-gelation through tissue using magnetically modulated optical nanoprobes (MagMOONs)," Sens. Actuators, B **205**, 313–321 (2014).

[9]L. Baraban, M. Tasinkevych, M. N. Popescu, S. Sanchez, S. Dietrich, and O. G. Schmidt, "Transport of cargo by catalytic Janus micro-motors," Soft Matter **8**(1), 48–52 (2012).

[10]L. F. Valadares, Y.-G. Tao, N. S. Zacharia, V. Kitaev, F. Galembeck, R. Kapral, and G. A. Ozin, "Catalytic nanomotors: Self-propelled sphere dimers," Small **6**(4), 565–572 (2010).

[11]R. Golestanian, T. B. Liverpool, and A. Ajdari, "Propulsion of a molecular machine by asymmetric distribution of reaction products," Phys. Rev. Lett. **94**(22), 220801 (2005).

[12]U. Bozuyuk, Y. Alapan, A. Aghakhani, M. Yunusa, and M. Sitti, "Shape anisotropy-governed locomotion of surface microrollers on vessel-like microtopographies against physiological flows," Proc. Natl. Acad. Sci. U. S.A. **118**(13), e2022090118 (2021).

[13]R. Streubel, V. P. Kravchuk, D. D. Sheka, D. Makarov, F. Kronast, O. G. Schmidt, and Y. Gaididei, "Equilibrium magnetic states in individual hemispherical permalloy caps," Appl. Phys. Lett. **101**(13), 132419 (2012).

[14]W. H. Meiklejohn and C. P. Bean, "New magnetic anisotropy," Phys. Rev. **105**(3), 904–913 (1957).

[15]J. Nogués and I. K. Schuller, "Exchange bias," J. Magn. Magn. Mater. **192**(2), 203–232 (1999).

[16]R. L. Stamps, "Mechanisms for exchange bias," J. Phys. D: Appl. Phys. **34**(3), 444 (2001).

[17]A. Tomita, M. Reginka, R. Huhnstock, M. Merkel, D. Holzinger, and A. Ehresmann, "Magnetic textures in hemispherical thin film caps with in-plane exchange bias," J. Appl. Phys. **129**(1), 015305 (2021).

[18]R. Micheletto, H. Fukuda, and M. Ohtsu, "A simple method for the production of a two-dimensional, ordered array of small latex particles," Langmuir **11**(9), 3333–3336 (1995).

[19]B. Gross, D. P. Weber, D. Rüffer, A. Buchter, F. Heimbach, A. Fontcuberta i Morral, D. Grundler, and M. Poggio, "Dynamic cantilever magnetometry of individual CoFeB nanotubes," Phys. Rev. B **93**(6), 064409 (2016).

[20]B. Gross, S. Philipp, E. Josten, J. Leliaert, E. Wetterskog, L. Bergström, and M. Poggio, "Magnetic anisotropy of individual maghemite mesocrystals," Phys. Rev. B **103**, 014402 (2021).

[21]T. Fischbacher, M. Franchin, G. Bordignon, and H. Fangohr, "A systematic approach to multiphysics extensions of finite-element-based micromagnetic simulations: Nmag," IEEE Trans. Magn. **43**(6), 2896–2898 (2007).

[22]A. Mehlin, B. Gross, M. Wyss, T. Schefer, G. Tütüncüoglu, F. Heimbach, A. Fontcuberta i Morral, D. Grundler, and M. Poggio, "Observation of end-vortex nucleation in individual ferromagnetic nanotubes," Phys. Rev. B **97**, 134422 (2018).

[23]A. Buchter, R. Wölbing, M. Wyss, O. F. Kieler, T. Weimann, J. Kohlmann, A. B. Zorin, D. Rüffer, F. Matteini, G. Tütüncüoglu, F. Heimbach, A. Kleibert, A. Fontcuberta i Morral, D. Grundler, R. Kleiner, D. Koelle, and M. Poggio, "Magnetization reversal of an individual exchange-biased permalloy nanotube," Phys. Rev. B **92**(21), 214432 (2015).

[24]A. Paul, C. Schmidt, N. Paul, A. Ehresmann, S. Mattauch, and P. Böni, "Symmetric magnetization reversal in polycrystalline exchange coupled systems via simultaneous processes of coherent rotation and domain nucleation," Phys. Rev. B **86**, 094420 (2012).

[25]A. Mourkas, A. Zarlaha, N. Kourkoumelis, and I. Panagiotopoulos, "Curvature induced stabilization of vortices on magnetic spherical sector shells," J. Magn. Magn. Mater. **524**, 167676 (2021).

[26]N. D. Müglich, A. Gaul, M. Meyl, A. Ehresmann, G. Götz, G. Reiss, and T. Kuschel, "Time-dependent rotatable magnetic anisotropy in polycrystalline exchange-bias systems: Dependence on grain-size distribution," Phys. Rev. B **94**, 184407 (2016).

[27]J. Geshev, L. G. Pereira, and J. E. Schmidt, "Rotatable anisotropy and coercivity in exchange-bias bilayers," Phys. Rev. B **66**, 134432 (2002).

[28]M. Merkel, R. Huhnstock, M. Reginka, D. Holzinger, M. Vogel, A. Ehresmann, J. Zehner, and K. Leistner, "Interrelation between polycrystalline structure and time-dependent magnetic anisotropies in exchange-biased bilayers," Phys. Rev. B **102**(14), 144421 (2020).

[29]J. Nogués, J. Sort, V. Langlais, V. Skumryev, S. Suriñach, J. S. Muñoz, and M. D. Baró, "Exchange bias in nanostructures," Phys. Rep. **422**(3), 65–117 (2005).

[30]R. Huhnstock, M. Reginka, A. Tomita, M. Merkel, K. Dingel, D. Holzinger, B. Sick, M. Vogel, and A. Ehresmann, "Translatory and rotatory motion of exchange-bias capped Janus particles controlled by dynamic magnetic field landscapes," Sci. Rep. **11**(1), 21794 (2021).